

TransCenter: Transformers with Dense Queries for Multiple-Object Tracking

Yihong Xu*, Yutong Ban*, Guillaume Delorme, Chuang Gan, Daniela Rus, *Fellow, IEEE*,
and Xavier Alameda-Pineda, *Senior Member, IEEE*

Abstract—Transformer networks [61] have proven extremely powerful for a wide variety of tasks since they were introduced. Computer vision is not an exception, as the use of transformers has become very popular in the vision community in recent years. Despite this wave, multiple-object tracking (MOT) exhibits for now some sort of incompatibility with transformers. We argue that the standard representation – bounding boxes with insufficient sparse queries – is not optimal to learning transformers for MOT. Inspired by recent research, we propose TransCenter, the first transformer-based MOT architecture for dense heatmap predictions. Methodologically, we propose the use of dense pixel-level multi-scale queries in a transformer dual-decoder network, to be able to globally and robustly infer the heatmap of targets' centers and associate them through time. TransCenter outperforms the current state-of-the-art in standard benchmarks both in MOT17 [43] and MOT20 [10]. Our ablation study demonstrates the advantage in the proposed architecture compared to more naive alternatives. The code will be made publicly available at <https://github.com/yihongxu/transcenter>.

Index Terms—Multiple-Object Tracking, Transformers, Dense Pixel-level Multi-Scale Queries, Dual Decoder.

1 INTRODUCTION

The task of tracking multiple objects, usually understood as the simultaneous inference of the positions and identities of various persons (trajectories) in a visual scene recorded by one or more cameras, became a core problem in computer vision in the past years. Undoubtedly, the various multiple-object tracking (MOT) challenges and associated datasets [10], [43], helped foster research on this topic and provided a standard way to evaluate and monitor the performance of the methods proposed by many research teams worldwide.

Recent progress in computer vision using transformers [61] for tasks such as pedestrian detection [7], [37], [78], person re-identification (Re-ID) [26] or image super resolution [69], showed the benefit of attention-based mechanisms and global receptive field. Transformers are good at modeling dependencies between different parts of an image and thus at taking global decisions. These advantages fit perfectly the underlying challenges of MOT, where current methods often struggle when modeling the interaction between people in crowded scenes. We, therefore, are very interested in investigating the use of transformer-based architectures for MOT, enabling global estimations when finding trajectories thus reducing missed or noisy tracks.

In the MOT community, using a bounding box to locate pedestrian is intuitive since bounding box is a wide-spread representation for MOT used in combination with probabilistic methods [2], [50] or deep convolutional architectures [3], [18], [47], [54], [64], [68], [71]. One of the prominent drawbacks of using bounding

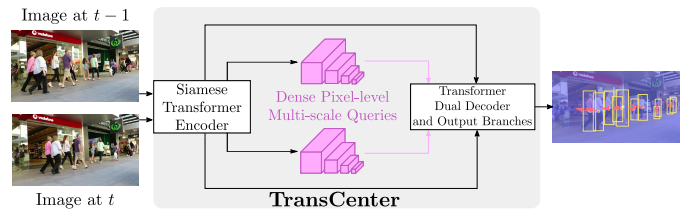


Fig. 1: Overview of our proposed pipeline¹: TransCenter replaces the sparse queries with dense pixel-level multi-scale queries to make sufficient and correct dense heatmap predictions. The predictions benefit from the long-range dependencies and global receptive field of transformers to interact with each other modeling the multi-object tracking task in a global way.

boxes for tracking multiple objects manifests when dealing with very crowded scenes [10], where occlusions are very difficult to handle since ground-truth bounding boxes often overlap each other. This is problematic because these bounding boxes are used during training, not only to regress the position, width, and height of each person but also to discriminate the visual appearance associated with each track. In this context, overlapping bounding boxes mean training a visual appearance representation that combines the visual content of two or even more people [24], [25]. Certainly, jointly addressing the person tracking and segmentation tasks [42] can partially solve the occlusion problem. However, this requires having extra annotations – segmentation masks – which are very tedious and costly to obtain. In addition, such annotations are not available in standard benchmark datasets [10], [43].

In this paper, we get inspiration from very recent research, demonstrating state-of-the-art performance before us, [72], [73], [76] to use dense center-based object heatmap representations, which are two-dimensional Gaussian distributions representing the objects' positions and sizes. We propose to investigate the use

- Y. Xu, G. Delorme, X. Alameda-Pineda are with Inria Grenoble Rhône-Alpes, Montbonnot Saint-Martin, France.
E-mail: {firstname.lastname}@inria.fr
- Y. Ban, D. Rus are with Distributed Robotics Lab, CSAIL, Massachusetts Institute of Technology.
E-mail: {yban, rus}@csail.mit.edu
- C. Gan is with MIT-IBM Watson AI Lab.
E-mail: ganchuang@csail.mit.edu

Y. Xu and Y. Ban contributed equally to this work.

1. the heatmap at $t - 1$ is omitted for simplicity, detailed in Fig. 2.

of transformer-based architectures with the dense center heatmap representation of each person and name our architecture as TransCenter. While this intuition is very straightforward, designing a powerful transformer-based architecture that implements this intuition is far from evident.

Indeed, the scientific challenge is to be able to infer dense representations (i.e. center heatmaps) with transformers. Directly combining existing MOT transformer-based architectures [7] and the center representation [76] does not work for two main reasons. First, fixed-size and insufficient sparse queries proposed in [7] are prone to miss detections and are not suitable for dense outputs. Simply increasing the number of queries causes overlapping and does not increase the overall tracking quality. Second, the objective of [7], [78] is to learn different object class representations in queries, which is *fundamentally different* from what we want to achieve: to learn if a pixel on a heatmap contains the person in the current/previous image. To overcome these limitations, we carefully design the network structure: we propose the use of dense pixel-level multi-scale queries. In addition, to allow heatmap-based MOT, the use of dense queries overcomes the limitations [7], [78] associated with querying the decoder with sparse queries to predict bounding boxes.

TransCenter is conceived to 1) solve the insufficient queries while keeping low false tracks for benefiting the long-range dependencies of transformers; 2) mitigate the occlusion problem inherent to anchor-based bounding-box tracking without requiring extra ground-truth annotations such as segmentation masks. Overall, this paper has the following contributions:

- We are among the first to show the benefits of using transformer-based architectures for MOT.
- We carefully explore different network structures to combine the transformer with center representations, specifically proposed *dense pixel-level multi-scale queries* that are mutually correlated within the transformer attention and produce *abundant but less noisy tracks*.
- We extensively compare with up-to-date online MOT tracking methods, TransCenter sets a *new state-of-the-art* baseline both in MOT17 [43] (+6.0% Multiple-Object Tracking Accuracy, MOTA) and MOT20 [10] (+8.7% MOTA) by a large margin, leading both MOT competitions by now in the published literature.

2 RELATED WORKS

2.1 Multiple-Object Tracking

In MOT literature, initial works [1], [2], [50] focus on how to find the optimal associations between detections and tracks through probabilistic models while [44] first formulates the problem as an end-to-end learning task with recurrent neural networks. Moreover, [52] models the dynamics of objects by a recurrent network and further combines the dynamics with an interaction and an appearance branch. [68] proposes a framework to directly use the standard evaluation measures MOTA and MOTP as loss functions to back-propagate the errors for an end-to-end tracking system. [3] employs object detection methods for MOT by modeling the problem as a regression task. A person Re-ID network [3], [60] can be added at the second stage to boost the performance. However, it is still not optimal to treat the Re-ID as a secondary task. [72] further proposes a framework that treats the person detection and Re-ID tasks equally and [45] uses quasi-dense proposals from

anchor-based detectors to learn Re-ID features for MOT in a dense manner. Motion clues in MOT are also important since a well-designed motion model can compensate for missing detections due to occlusions. To this end, [21], [53] focus on the motion-based interpolation based on probabilistic models. [62] unifies the segmentation and detection task in an MOT framework combining historic tracking information as a strong clue for the data association. Derived from the success in single-object tracking, [56] employs siamese networks for MOT. Moreover, traditional graphs are also used to model the positions of objects as nodes and the temporal connection of the objects as edges [27], [31], [58], [59], [60]. The performance of those methods is further boosted by the recent rise of Graph Neural Networks (GNNs): hand-designed graphs are replaced by learnable GNNs [6], [22], [46], [64], [65], [66] to model the complex interaction of the objects.

Most of the above methods follow the tracking by detections/regression paradigm where a detector provides detections for tracking. The paradigm has been proven state-of-the-art performance with the progress in object detectors. However, the anchor box-based representation is not a satisfying solution because it creates ambiguity when objects occlude each other, or noisy background information is included. Unlike classic anchor-based detectors [48], [49], recent progress in keypoint-based detectors [33], [77] exhibited better performance while discarding overlapping and manually-designed box anchors trying to cover all possible object shapes and positions. Built on keypoint-based detectors, [76], [72] and [73] represent objects as centers in a heatmap then reason about all the objects jointly and associate them across adjacent frames with a tracking branch or Re-ID branch.

2.2 Transformers in Vision

Transformer is first proposed by [61] for machine translation, and has shown its ability to handle long-term complex dependencies between sequences by using multi-head attention mechanism. With its great success in natural language processing, works in computer vision start to investigate transformers for various tasks, such as image recognition [14], Person Re-ID [26], realistic image generation [29], super resolution [69] and audio-visual learning [16], [17].

Object detection with Transformer (DETR) [7] can be seen as an exploration and correlation task. It is an encoder-decoder structure where the encoder extracts the image information and the decoder finds the best correlation between the object query and the encoded image features with an attention module. However, the attention calculation suffers from heavy computational and memory complexities w.r.t the input size: the feature maps extracted from a ResNet [23] backbone are used to alleviate the problem. Deformable DETR [78] further solves the issue by proposing deformable attention inspired by [9], drastically speeding up the convergence ($10\times$) and reducing the complexity. The reduction of memory consumption allows in practice using multi-scale features to capture finer details, yielding better detection performance.

Before transformers, some simple attention-based modules have been introduced for MOT. Specifically, [20] proposes a target and distractor-aware attention module to produce more reliable appearance embeddings, which also helps suppress detection drift and [63] proposes hand-designed spatial and temporal correlation modules to achieve long-range information similar to what transformers inherit. After the success in detection using transformers,

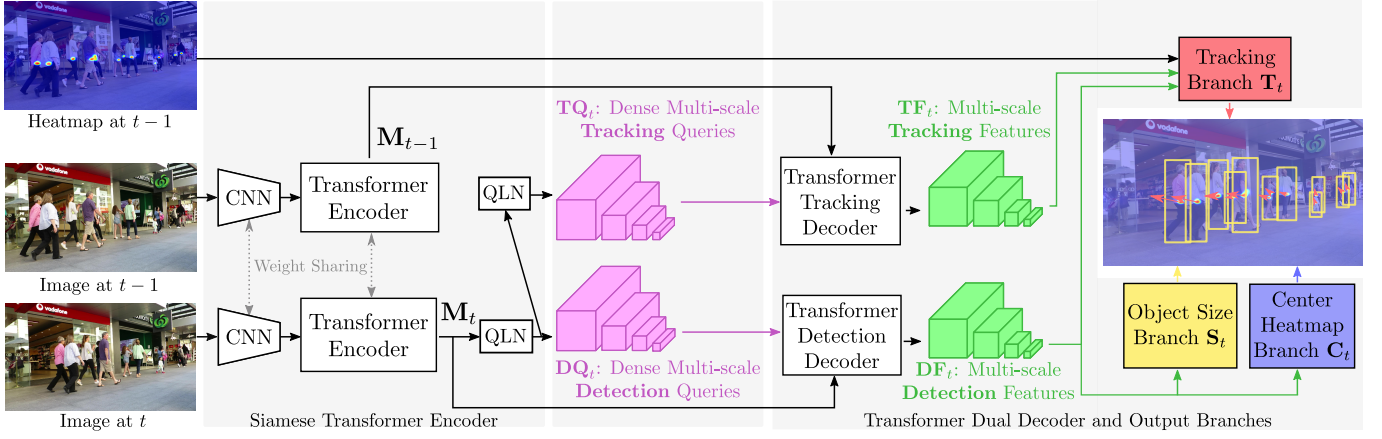


Fig. 2: Overview of TransCenter. Images at t and $t - 1$ are fed to a CNN backbone to produce multi-scale features, then processed by a deformable transformer encoder to produce memories M_t and M_{t-1} respectively. M_t is used to compute dense pixel-level multi-scale detection and tracking queries (DQ_t and TQ_t) through two query learning networks (QLNs). DQ_t and TQ_t are fed to the detection and tracking deformable transformer decoder respectively, together with M_t and M_{t-1} . The outputs are multi-scale detection and tracking features (DF_t and TF_t) and are used to estimate the center heatmap and object sizes. Both multi-scale features (DF_t and TF_t), together with the center heatmap at $t - 1$, C_{t-1} are used to estimate image size displacement heatmap T_t indicating for each center at t their displacement to $t - 1$ (red arrows).

two concurrent works directly apply transformers on MOT based on (deformable) DETR framework. First, Trackformer [42] builds directly from DETR [7] and is trained to propagate the queries through time. Second, Transtrack [57] extends [78] to MOT by adding a decoder that processes the features at $t - 1$ to refine previous detection positions. Importantly, both methods stay in the DETR framework with sparse queries and extend it for tracking, a strategy that has been proven successful in previous works [3], [68]. However, recent literature [72], [73], [76] also suggests that point-based tracking may be a better option for MOT while the use of pixel-level dense queries with transformers to predict dense heatmaps for MOT has never been studied. All above motivates us to investigate a better transformer-based MOT framework with careful designs considering existing drawbacks, thus introducing TransCenter achieving state-of-the-art performance.

3 TRANSFORMER BACKGROUNDS

The proposed model has been inspired by the object-detection framework DETR [7]. In this section, we briefly recall the DETR framework and the attention basis in transformers, illustrated in Fig. 3. DETR framework consists of a CNN backbone, a transformer-based encoder-decoder, an object detection and classification module. The detailed pipeline is described as follows: First of all, given the features $f \in \mathcal{R}^{H \times W \times C}$ generated by a CNN backbone (i.e. ResNet [23]), DETR collapses the spatial dimension to $f \in \mathcal{R}^{HW \times C}$, since sequential inputs are required for transformers. Secondly, the transformer encoder takes the sequential feature maps as input and generates a memory M , which contains the information of the inter-correlation between the feature maps (Self-Attention). Thirdly, a set of learnable queries are designed, where each query corresponds to a possible object/background in the image. Then the transformer decoder tries to explore the correlation between the learnable queries and the encoded memory M (Cross-Attention). Lastly, as final outputs, the output of the transformer decoder are fed into a simple multi-layer perceptron (MLP) to predict a bounding box and a class probability per query telling if the box corresponds to an

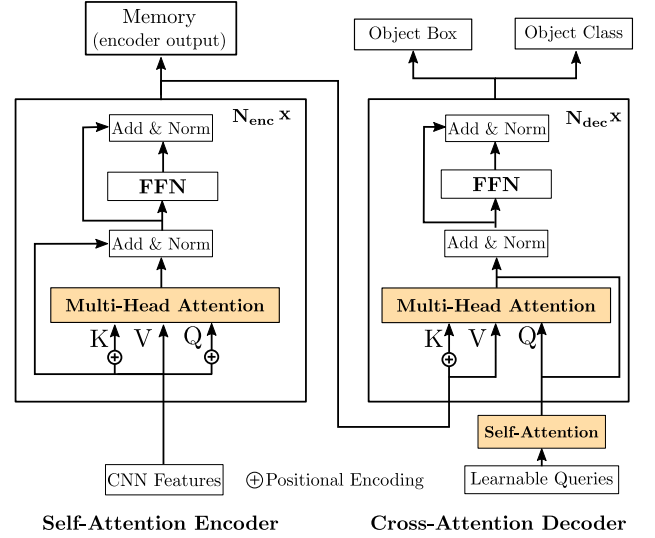


Fig. 3: DETR framework.

object. Inside each transformer (encoder/decoder), the correlation are operated in several transformer layers concatenated ($N_{enc} = N_{dec} = 6$) sequentially and each layer contains several multi-head attention modules (deformable attention in [78]) processing in parallel. The attention module computes the attention map by calculating:

$$\text{Attention}(Q, K, V) = \text{Softmax}\left(\frac{QK^T}{\sqrt{h}}\right)V \quad (1)$$

where Q, K, h is the query, the key, and the hidden dimension, respectively. And the value V is followed by feed-forward networks, skip connections, and normalization layers to produce an attended output. In practice, Q, K, V are generated from the CNN feature maps for the encoder. For the decoder, Q is from randomly initialized learnable queries and K, V are from the encoder memory M .

4 METHODOLOGY

MOT is a more complex task both detecting objects and associating them correctly across frames. DETR has demonstrated its power with transformers for object detection, which motivates us to investigate the use of transformers for MOT. However, we question the direct transfer from DETR to MOT as concurrent works do [42], [57]. As visualized in Fig. 7 and discussed in Sec. 5.4, the sparse queries without positional correlations are problematic in two folds: First, the insufficient number of queries will cause severe miss detections thus false negatives (FNs) in tracking. Second, queries are highly overlapping, and simply increasing the number of non-positional-correlated queries may end up having many false detections then false positives (FPs) in tracking. Therefore, to solve the two issues, we introduce the use of *dense pixel-level multi-scale queries* (see details in Sec. 4.2) combining with transformers to perform MOT. Up to our knowledge, we are the first to propose the use of a dense query feature map that scales with the input image size for MOT leveraging transformers. To give a figure, in our experiments the dual-decoder is queried with roughly 14k queries. Indeed, one downside of using dense queries is the associated memory consumption. To mitigate this undesirable effect, we propose to use deformable transformers [78] for both the encoder and the dual-decoder.

For the dual-decoder, as detailed in Sec. 4.1 and Sec. 4.3, we cast the MOT problem into two separate sub-tasks: the detection of objects at time t , and the association with objects detected at $t - 1$. Different from previous studies following the same rationale [3], [68], TransCenter addresses these two tasks in parallel, by using a fully deformable dual decoder architecture. Instead of sparse bounding-box predictions, with dense pixel-level queries, the output of the detection decoder is used to estimate the object center and the size heatmap, while it is combined with the output of the tracking decoder to estimate the displacement of the object w.r.t. the previous image (see Sec. 4.4).

4.1 TransCenter in a Nutshell

The overall architecture of TransCenter can be seen in Fig. 2. Deformable transformers [78] are used in the encoder and the dual-decoder respectively to extract self-dependencies of images' feature maps and correlations of dense queries and encoded features from the outputs of the encoder (positional encoding is kept as [78]). Precisely, the RGB images at time t and $t - 1$ are fed to a CNN backbone to produce multi-scale features that capture finer details in the image. The features are input to a (share-weight) deformable self-attention transformer encoder in a siamese way, thus obtaining *multi-scale* memory feature maps, \mathbf{M}_t and \mathbf{M}_{t-1} , associated to the two images respectively. The multi-scale attribute will be inherited by the pixel-level dense queries: \mathbf{M}_t is given to a query learning network (QLN), consisting of 2 fully-connected layers with ReLU activation and skip connections operating in the feature dimension (channel dimension changes from 256 to 512 and then back to 256), which output dense multi-scale detection queries, \mathbf{DQ}_t . These go through another QLN to produce a feature map of dense multi-scale tracking queries, \mathbf{TQ}_t . A fully deformable transformer dual decoder architecture is then used to process them: the deformable detection decoder correlates the detection queries \mathbf{DQ}_t with \mathbf{M}_t to output multi-scale detection features \mathbf{DF}_t , and the deformable transformer tracking decoder does the same but with the tracking queries \mathbf{TQ}_t and \mathbf{M}_{t-1} .

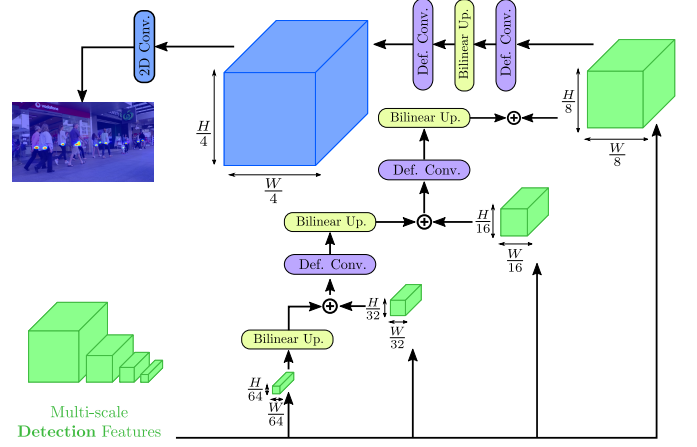


Fig. 4: Overview of the center heatmap branch. The multi-scale detection features are up-scaled and merged via a series of deformable convolutions [9], into the output center heatmap. A similar strategy is followed for the object size and the tracking branches.

to output multi-scale tracking features \mathbf{TF}_t . \mathbf{DF}_t are used to estimate the bounding box size \mathbf{S}_t and the center heatmap \mathbf{C}_t . Together with \mathbf{DF}_t and the center heatmap, \mathbf{C}_{t-1} , \mathbf{TF}_t are used to estimate the tracking displacement \mathbf{T}_t .

In the following we first explain the design of the pixel-level dense multi-scale queries, then the architecture of the fully deformable dual decoder, the output branches – center heatmap, object size, and tracking – and finally the training losses.

4.2 Pixel-Level Dense Multi-scale Queries

Traditional transformer architectures output as many elements as queries fed to the decoder, and more importantly, these outputs correspond to the entities sought (e.g. pedestrian bounding boxes). As observed in Fig. 7 and discussed in the experiment section 5.4, insufficient sparse queries are problematic and dense queries can provide sufficient outputs. However, naively introducing the dense queries is dangerous because if they are highly overlapping, the queries are redundant and may cause FPs. To solve the issue, we propose to use dense pixel-level queries without overlapping to produce dense heatmaps, inferring the probability of having a person's center at a given pixel coordinate. We recall that such queries are multi-scale obtained from the multi-scale \mathbf{M}_t , via a first QLN obtaining \mathbf{DQ}_t . We use two different queries for the dual decoder: a second QLN processes \mathbf{DQ}_t to obtain \mathbf{TQ}_t . They will be fed to the fully dual deformable transformer decoder, see Sec. 4.3.

The fact that the dense query feature map resolution is proportional to the resolution of the input image has three prominent advantages. First, the queries are multi-scale and exploit the multi-resolution structure of the encoder, allowing for very small targets to be captured by those queries. Second, dense queries also make the network more flexible since it can adapt *automatically* to arbitrary image size without re-parameterizing. Third, the query-pixel correspondence *discards the time-consuming Hungarian matching* for the query-ground-truth object association during training. More generally, the use of QLN avoids the problem of manually sizing the queries and selecting beforehand the number of maximum detection, as it was done in previous transformer architectures (for computer vision).

4.3 Fully Deformable Dual Decoder

To successfully find object trajectories, an MOT method should not only detect the objects but also associate them across frames. To do so, TransCenter proposes to use a fully deformable dual decoder. More precisely, two fully deformable decoders deal in parallel with the two subtasks: detection and tracking. While the detection decoder correlates \mathbf{DQ}_t and \mathbf{M}_t with the attention modules to detect objects in the image I_t , the tracking decoder correlates \mathbf{TQ}_t and \mathbf{M}_{t-1} to displace the detected objects to their positions in the previous image I_{t-1} . Specifically, the detection decoder searches for objects in multi-scale \mathbf{M}_t with the attention correlated to the multi-scale \mathbf{DQ}_t and then outputs \mathbf{DF}_t , used to find the object centers and box sizes. Differently, the deformable tracking decoder finds the objects in \mathbf{M}_{t-1} and associates them with the objects at t . To do this, the multi-head deformable attention in the tracking decoder performs a temporal cross-correlation between the multi-scale \mathbf{TQ}_t and \mathbf{M}_{t-1} and outputs the multi-scale tracking features \mathbf{TF}_t , containing the temporal information that is used in the tracking branch to estimate the displacements from time t back to $t - 1$.

Both the detection and tracking decoders input a dense query feature map to output dense information as well. However, the use of the multi-head attention modules used in traditional transformers [61] in TransCenter implies a memory and complexity growth that is quadratic with the input image size $O(H^2W^2)$. Of course, this is undesirable and would limit the scalability and usability of the method, especially when processing multi-scale features. To mitigate this, we resort to deformable multi-head attention [78], thus leading to a fully deformable dual decoder architecture as the deformable encoder.

4.4 The Center, the Size and the Tracking Branches

The outputs of the dual-decoder are two sets of multi-scale features, referred to as the detection \mathbf{DF}_t and tracking features \mathbf{TF}_t . More precisely, these multi-scale features contain four feature maps at different resolutions, namely $1/64, 1/32, 1/16$, and $1/8$ of the input image resolution. For the center heatmap and the object size and tracking branches, the feature maps at different resolutions are combined using deformable convolutions [9] and bilinear interpolation, following the architecture shown in Fig. 4, into a feature map of $1/4$ of the input resolution, and finally into $\mathbf{C}_t \in [0, 1]^{H/4 \times W/4}$ (H and W are the input image height and width, respectively) and $\mathbf{S}_t \in \mathbb{R}^{H/4 \times W/4 \times 2}$ (the two channels of \mathbf{S}_t encode the object width and the height). Regarding the tracking branch, the two multi-scale features (\mathbf{DF}_t and \mathbf{TF}_t) follow the same up-scaling as in the two other branches (but with different parameters), obtaining two feature maps at resolution $1/4$ of the input resolution. These two feature maps are concatenated to the previous center heatmap \mathbf{C}_{t-1} downscaled to the resolution of the feature maps. As in the other branches, a block of convolutional layers computes the final output, i.e. the displacement of the objects $\mathbf{T}_t \in \mathbb{R}^{H/4 \times W/4 \times 2}$ where the two channels encode the horizontal and vertical displacements respectively.

4.5 Training TransCenter

Training TransCenter is achieved by jointly learning a 2D classification task for the object center heatmap and a regression task for the object size and tracking displacements, covering the branches of TransCenter. For the sake of clarity, in this section, we will drop the time index t .

Center Focal Loss In order to train the center branch, we need first to build the ground-truth heatmap response $\mathbf{C}^* \in [0, 1]^{H/4 \times W/4}$. As done in [76], we construct \mathbf{C}^* by considering the maximum response of a set of Gaussian kernels centered at each of the $K > 0$ ground-truth object centers. More formally, for every pixel position (x, y) the ground-truth heatmap response is computed as:

$$\mathbf{C}_{xy}^* = \max_{k=1, \dots, K} G((x, y), (x_k, y_k); \sigma), \quad (2)$$

where (x_k, y_k) is the ground-truth object center, and $G(\cdot, \cdot; \sigma)$ is the Gaussian kernel with spread σ . In our case, σ is proportional to the object's size, as described in [33]. Given the ground-truth \mathbf{C}^* and the inferred \mathbf{C} center heatmaps, the center focal loss, L_C is formulated as:

$$L_C = \frac{1}{K} \sum_{xy} \begin{cases} (1 - \mathbf{C}_{xy})^\alpha \log(\mathbf{C}_{xy}) & \mathbf{C}_{xy}^* = 1, \\ (1 - \mathbf{C}_{xy}^*)^\beta (\mathbf{C}_{xy})^\alpha \log(1 - \mathbf{C}_{xy}) & \text{otherwise.} \end{cases} \quad (3)$$

where the scaling factors are $\alpha = 2$ and $\beta = 4$, see [72].

Sparse Regression Loss The values of \mathbf{S} and \mathbf{T} are supervised only on the locations where object centers are present, i.e. $\mathbf{C}_{xy}^* = 1$ using a L_1 loss:

$$L_S = \frac{1}{K} \sum_{xy} \begin{cases} \|\mathbf{S}_{xy} - \mathbf{S}_{xy}^*\|_1 & \mathbf{C}_{xy}^* = 1, \\ 0 & \text{otherwise.} \end{cases} \quad (4)$$

The formulation of L_T is analogous to L_S but using the tracking output and ground-truth, instead of the object size. To complete the sparsity of L_S , L_T , we add an extra L_1 regression loss, denoted as L_R with the bounding boxes computed from \mathbf{S}_t and ground-truth centers. The impact of this additional loss is marginal as shown in Section 5.4.

In summary, the overall loss is formulated as the weighted sum of all the losses, the weights are chosen according to the numeric scale of each loss:

$$L = L_C + \lambda_S L_S + \lambda_T L_T + \lambda_R L_R \quad (5)$$

5 EXPERIMENTAL EVALUATION

5.1 Implementation Details

Inference with TransCenter Once the method is trained, we detect objects by filtering the output center heatmap \mathbf{C}_t . Since the datasets are annotated with bounding boxes, we need to convert our estimates into this representation. In detail, we apply a threshold $\tau = 0.5$ to the heatmap, thus producing a list of center positions $\{\mathbf{c}_{t,k}\}_{k=1}^{K_t}$. We extract the object size $\mathbf{s}_{t,k}$ associated to each position $\mathbf{c}_{t,k}$ in \mathbf{S}_t . The set of detections produced by TransCenter is directly $\mathbf{D}_t = \{\mathbf{c}_{t,k}, \mathbf{s}_{t,k}\}_{k=1}^{K_t}$. Once the detection step is performed, we can estimate the position of the object in the previous image extracting the estimated displacement $\mathbf{t}_{t,k}$ from the tracking branch output \mathbf{T}_t and the center position $\mathbf{c}_{t,k}$. Indeed, we can construct a set of detections *tracked back to the previous image* $\hat{\mathbf{D}}_{t-1} = \{\mathbf{c}_{t,k} + \mathbf{t}_{t,k}, \mathbf{s}_{t,k}\}_{k=1}^{K_t}$. Finally, we use \mathbf{T}_t and the Hungarian algorithm to match the detections at the previous time step \mathbf{D}_{t-1} with the tracked-back detection $\hat{\mathbf{D}}_{t-1}$ to associate the tracks through time. The birth and death processes are naturally integrated in TransCenter: Detections not associated to previous detections give birth to new tracks, while unmatched previous detections are put to sleep for at most $T = 60$ frames before being discarded. New tracks are compared to sleeping tracks by means

TABLE 1: Results on MOT17 testset. The left and right halves of the table correspond to public and private detections respectively. The cell background color encodes the amount of extra-training data: green for none, orange for one extra dataset, red for five extra datasets. Methods with * are not associated to a publication. The best result within the same training conditions (background color) is underlined. The best result among published methods is in **bold**. Best seen in color.

	Public Detections									Private Detections																	
Method	Data	MOTA ↑	MOTP ↑	IDF1 ↑	MT ↑	ML ↓	FP ↓	FN ↓	IDS ↓	Data	MOTA ↑	MOTP ↑	IDF1 ↑	MT ↑	ML ↓	FP ↓	FN ↓	IDS ↓									
TransCenter (Ours)	CH	71.9	81.4	62.3	38.0	22.7	17,378	137,008	4,046	CH	73.2	81.1	62.2	40.8	18.5	23,112	123,738	4,614									
SiamMOT [56]	CH	65.9		63.5	34.6	23.9	18,098	170,955	3,040																		
*TrackFormer [42]	CH	61.8		59.8	35.4	21.1	35,226	177,270	2,982																		
GMT_CT [22]	RE2	61.5	66.9	26.3	32.1	14,059	200,655	2,415																			
*UnsupTrack [30]	PT	61.7	78.3	58.1	27.2	32.4	16,872	197,632	1,864																		
MOTDT17 [8]	RE1	50.9	76.6	52.7	17.5	35.7	24,069	250,768	2,474																		
TraDeS [62]																											
*TransTrack [57]																											
CenterTrack [76]	NO	61.5	78.9	59.6	26.4	31.9	14,076	200,672	2,583										CH	67.8	78.4	64.7	34.6	24.6	18,489	160,332	3,039
*FUFET [54]	NO	62.0		59.5	27.8	31.5	15,114	19,6672	2,621										(5D1)	76.2	81.1	68.0	51.1	13.6	32,796	98,475	3,237
MLT [71]																			(5D1)	75.3	81.7	75.5	49.3	19.5	27,879	109,836	1,719
*CSTrack [36]										5D1	74.9	80.9	72.6	41.5	17.5	23,847	114,303	3,567									
*FairMOT [72]										5D1	73.7	81.3	72.3	43.2	17.3	27,507	117,477	3,303									
SOTMOT [73]	5D1	62.8		67.4	24.4	33.0	6,556	201,319	2,017	5D1	71.0		71.9	42.7	15.3	39,537	118,983	5,184									
CorrTracker [63]										5D2	76.5		73.6	47.6	12.7	29,808	99,510	3,369									
GSDT_V2 [64]										5D2	73.2		66.5	41.7	17.5	26,397	120,666	3,891									
GSDT [64]										5D2	66.2	79.9	68.7	40.8	18.3	43,368	144,261	3,318									
TetrD17 [68]	NO	53.7	77.2	53.8	19.4	36.6	11,731	247,447	1,947																		
Tracker [3]	NO	53.5	78.0	52.3	19.5	36.6	12,201	248,047	2,072																		
Tracker++ [3]	NO	56.3	78.8	55.1	21.1	35.3	8,866	235,449	1,987																		
GSM_Tractor [39]	NO	56.4	77.9	57.8	22.2	34.5	14,379	230,174	1,485																		
TADAM [20]	NO	59.7		58.7			9,676	21,6029	1,930																		
ArTIST-C [53]	NO	62.3		59.7	29.1	34.0	19,611	191,207	2,062																		
*MAT [21]	NO	67.1	80.8	69.2	38.9	26.4	22,756	161,547	1,279																		
MTP [32]	NO	51.5		54.9	20.5	35.5	29,623	241,618	2,563																		
ChainedTracker [47]																											
QDTrack [45]	NO	64.6	79.6	65.1	32.3	28.3	14,103	18,2998	2,652										NO	55.9		60.4	20.5	36.7	8,653	238,853	1,188
										NO	66.6	78.2	57.4	32.2	24.2	22,284	160,491	5,529									
										NO	68.7	79.0	66.3	40.6	21.9	26,589	14,6643	3,378									
TransCenter (Ours)	NO	68.8	79.9	61.4	36.8	23.9	22,860	149,188	4,102	NO	70.0	79.6	62.1	38.9	20.4	28,119	136,722	4,647									

of an external Re-ID network from [3] trained only on MOT17, whose impact is ablated in the experiments.

Network and Training Parameters The input images are resized to 640×1088 . Both the encoder and the decoder have six layers with hidden dimension $h = 256$ with eight attention heads. The query learning networks (QLN) consist of two fully connected layers with ReLU activation. Our CNN backbone is ResNet-50 [23]. TransCenter is trained with loss weights $\lambda_S = 0.1$, $\lambda_R = 0.5$ and $\lambda_T = 1.0$ by the AdamW optimizer [40] with learning rate $2e-5$ for the CNN backbone and $2e-4$ for the rest of the network. The training converges 50 epochs *instead of 150 reported in [57] and 400 epochs in [42]*, applying learning rate decay of $1/10$ at the 40th epoch. The entire network is pre-trained on the pedestrian class of COCO [38] and then fine-tuned on the respective MOT dataset [10], [43]. Overall, with 2 RTX Titan GPUs, batch size 2 each and around 20 GB of memory, it takes around 1h30 and 1h per epoch of MOT20 and MOT17 respectively. We also present the results fine-tuning with extra data, namely the CrowdHuman dataset [55]. See the results and discussion for details.

5.2 Protocol

Datasets and Detections We use the standard split of the MOT17 [43] and MOT20 [10] datasets and the evaluation is obtained by submitting the results to the MOTChallenge website. The MOT17 testset contains 2,355 trajectories distributed in 17,757 frames. MOT20 testset contains 1,501 trajectories within only 4,479 frames, which leads to a much more challenging setting. We evaluate TransCenter both under public and private detections. When using public detections, we limit the maximum number of birth candidates at each frame to be the number of

public detections per frame, as in [42], [76]. The selected birth candidates are those closest to the public detections with IOU larger than 0. When using private detections, there are no constraints, and the detections depend only on the network capacity, the use of external detectors, and more importantly, the use of extra training data. For this reason, we regroup the results by the use of extra training datasets as detailed in the following.

Extra Training Data To fairly compare with the state-the-art methods, we clearly denote the extra data used to train each method (including several pre-prints listed in the MOTChallenge leaderboard, which are marked with * in our result tables):² CH for CrowdHuman [55], PT for PathTrack [41], RE1 for the combination of Market1501 [74], CUHK01 and CUHK03 [34] person re-identification datasets, RE2 replaces CUHK01 [34] with DukeMTMC [51], 5d1 for the use 5 extra datasets (CrowdHuman, Caltech Pedestrian [12], [13], CityPersons [70], CUHK-SYS [67], and PRW [75]), 5d2 is the same as 5d1 replacing CroudHuman by ETH [15], (5d1) uses the tracking/detection results of FairMOT (trained with in 5d1 setting), and NO for using no extra dataset.

Metrics Standard MOT metrics such as MOTA (Multiple Object Tracking Accuracy) and MOTP (Multiple Object Tracking Precision) [4] are used: MOTA is mostly used since it reflects the average tracking performance including the number of FPs (False positives, predicted bounding boxes not enclosing any object), FNs (False negatives, missing ground-truth objects) and IDS [35] (Identities of predicted trajectories switch through time). MOTP evaluates the quality of bounding boxes from successfully tracked objects. Moreover, we also evaluate on IDF1 [51] (the ratio of correctly identified detections over the average number of ground-

2. COCO [38] and ImageNet [11] are not considered as extra data according to the MOTchallenge [10], [43].

TABLE 2: Results on MOT20 testset. The table is structured following the same principles as Tab. 1. Methods with * are not associated to a publication. The best result within the same training conditions (background color) is underlined. The best result among published methods is in **bold**. Best seen in color.

Method	Public Detections									Private Detections								
	Data	MOTA ↑	MOTP ↑	IDF1 ↑	MT ↑	ML ↓	FP ↓	FN ↓	IDS ↓	Data	MOTA ↑	MOTP ↑	IDF1 ↑	MT ↑	ML ↓	FP ↓	FN ↓	IDS ↓
TransCenter (Ours)	CH	62.3	79.9	50.3	48.8	15.8	43,006	147,505	4,545	CH	61.9	79.9	50.4	49.4	15.5	45,895	146,347	4,653
*UnsupTrack [30]	PT	53.6	<u>80.1</u>	<u>50.6</u>	30.3	25.0	6,439	231,298	2,178	5D2	67.1	<u>79.1</u>	67.5	53.1	13.2	31,913	135,409	3,131
GSDT [64]										5D2	67.1		67.5	53.1	13.2	31,507	135,395	3,230
GSDT_V2 [64]										5D2	65.2		69.1	66.4	8.9	79,429	95,855	5,183
CorrTracker [63]										5D1	68.6		71.4	64.9	9.7	57,064	101,154	4,209
SOTMOT [73]										5D1	66.6	78.8	68.6	50.4	15.5	<u>25,404</u>	144,358	3,196
*CSTrack [36]										5D1	61.8	78.6	67.3	<u>68.8</u>	<u>7.6</u>	<u>103,440</u>	<u>88,901</u>	5,243
*FairMOT [72]																		
SORT [5]	NO	42.7	78.5	45.1	16.7	26.2	27,521	264,694	4,470									
Tracker++ [3]	NO	52.6	79.9	52.7	29.4	26.7	6,930	236,680	1,648									
ArtIST-T [53]	NO	53.6		51.0	31.6	28.1	7,765	230,576	1,531									
*GNNMatch [46]	NO	54.5	79.4	49.0	32.8	25.5	9,522	223,611	2,038									
TADAM [20]	NO	56.6		51.6			39,407	18,2520	2,690									
MLT [71]																		
TransCenter (Ours)	NO	61.0	79.5	49.8	48.4	15.5	49,189	147,890	4,493	NO	60.6	79.5	49.6	48.6	15.4	52,332	146,809	4,604

truth objects and predicted tracks), MT (the ratio of ground-truth trajectories that are covered by a track hypothesis more than 80% of their life span), and ML (less than 20% of their life span).

5.3 Results and Discussion

MOT17 Tab. 1 presents the results obtained on the MOT17 testset. The first global remark is that most state-of-the-art methods do not evaluate under both public and private detections, and under different extra-training data settings, while we do. Secondly, TransCenter *systematically outperforms all other methods*, in terms of MOTA, under similar training data conditions, both for public and private detections. Precisely, the increase of MOTA w.r.t. the stage-of-the-art methods is of 6.0% (including unpublished methods by now) and 4.2% (1.7% including unpublished methods) for public detections under extra and no-extra training data, and of 4.1% and 1.3% for private detections. If we consider only published methods, the superiority of TransCenter is remarkable in most of the metrics. We can also observe that TransCenter trained with no extra-training data outperforms, not only the methods trained with no extra data but also some methods trained with one extra dataset (in terms of MOTA for both public and private detections). In the same line, TransCenter trained on CH performs better than two of the methods trained with five extra datasets. Overall, these results confirm our hypothesis that TransCenter with heatmap representations produced by global relevant pixel-level queries in transformers is a better choice.

MOT20 Tab. 2 reports the results obtained in MOT20 testset. In public detections, as in MOT17, TransCenter *leads the competition compared to all the other methods* both in extra (+8.7% MOTA) and no-extra (+4.4% MOTA) training data. Another remarkable achievement of TransCenter is the significant decrease of FP when compared to the existing methods ($-83\ k/-34\ k$ and beyond with/without extra training data). Very importantly, to the best of our knowledge, our study is the first to report the results on MOT20 of a transformer-based architecture, demonstrating the tracking capacity of TransCenter even in a densely crowded scenario. For private detections, both trained only on MOT, we outperform [71] by a large margin (+11.7%). Finally, for the sake of completeness, we provide the results on MOT20 for private detections and set a new baseline for future research for methods trained under CH.

Compared to Transformer-Based MOT With the scientific purpose and the respect to our *concurrent works*, we compare with them in standard datasets. Unfortunately, transformer-based methods [42], [57] by far only show results on MOT17. Using the same training strategy and data, we significantly outperform [57] by +7.4% MOTA, and [42] by +10.1% MOTA. Moreover, we recall that, unlike our concurrent works, TransCenter leverages pixel-level dense and multi-scale queries to predict dense point-based heatmaps, mitigating the miss-tracking problem.

Compared to Center-Based MOT With the long-term dependencies and larger receptive field of transformers, unlike pure CNN-based center MOT methods, our queries interact globally with each other and make global decisions, allowing TransCenter to exhibit superior performance compared to previous center-based MOT methods [72], [73], [76]. The benefits are two-fold: precisely, shown in Tab. 1, TransCenter *tracks more and better* compared to [76], with +5.4% (+7.3%) MOTA and -36,594 (-51,484) FNs in MOT17 private (public) detections, *using the same dense center representations trained with the same data*. Similar to [76], FairMOT closed up the gap of miss detections by training with much more data, leading to much fewer FNs but producing much noisier detections. Surprisingly, with much less training data, TransCenter still outperforms [72] (+0.1% MOTA) in very crowded MOT20 and has better FP-FN balance (-99) with *cleaner detections and better tracking associations* (-590 IDS). Similarly, a gain of 9.1% MOTA and -53,489 FN-FP balance are observed in MOT17 public detections with TransCenter trained only additionally on CH compared to [73] trained on 5D1. The above comparisons have demonstrated that our transformer-based center MOT exhibits significant superior performance.

5.4 Ablation Study

In this section, first, we experimentally demonstrate the importance of our proposed multi-scale pixel-level dense queries in TransCenter (see Fig. 5 and Tab. 3). Then, we justify the effectiveness of different configurations of our design for TransCenter (see Fig. 6 and Tab. 4). For the ablation, we divide the training sets into train-validation split, we take the first 50% of frames (2,664 and 4,468 frames for MOT17 and MOT20, respectively) as training data and test on the last 25% (1,332 and 2,234 frames for MOT17 and MOT20, respectively). The rest 25%

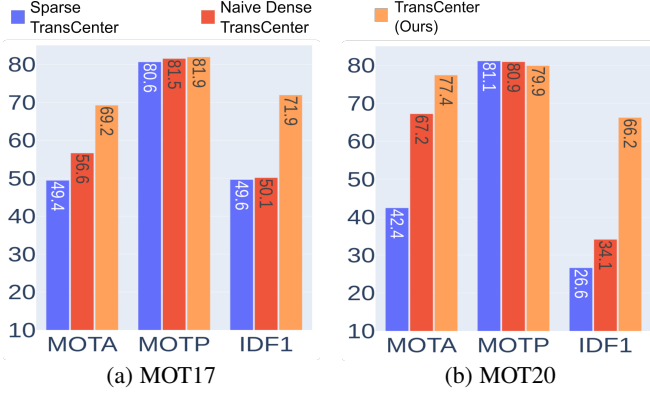


Fig. 5: Comparison of naive implementations of TransCenter using sparse (dense) queries and the proposed TransCenter in MOTA, MOTP and IDF1 tested on both MOT17 and MOT20 validation sets.

TABLE 3: Comparison of naive implementations of TransCenter using sparse (dense) queries and the proposed TransCenter tested on MOT17 and MOT20 in FP, FN and IDS.

Method	MOT17			MOT20		
	FP ↓	FN ↓	IDS ↓	FP ↓	FN ↓	IDS ↓
Sparse TransCenter	4,909	8,202	602	19,229	153,403	4,513
Naive Dense TransCenter	3,510	7,577	678	41,429	52,028	7,620
TransCenter (ours)	1,202	6,951	203	10,896	57,145	1,651

frames in the middle of the sequences are thrown to prevent overfitting. All the models are pre-trained on CrowdHuman and tested in private detections.

Dense Queries Are Necessary We implemented the transformer encoder, detection and tracking decoders as TransCenter but with sparse learnable queries to predict box centers and box sizes of objects as [78], namely Sparse TransCenter. From the results shown in Fig. 5 and Tab. 3, we see (Sparse v.s. Naive Dense TransCenter) that the limited number of queries (100, by default in [78]) is insufficient for detecting and tracking objects, especially in very crowded scenes MOT20 (+101,375 FNs, -24.8% MOTA).

Naive Dense TransCenter v.s. TransCenter One naive way to alleviate the insufficient queries is to greatly increase the number of queries like in Naive Dense TransCenter : we drastically increase the number of queries from 100 to 43,520 (i.e. $H/4 \times W/4$), same as the dense output of TransCenter. We note that TransCenter has 14,450 queries (i.e. the sum of the 1/8, 1/16, 1/32, and 1/64 of the image size) and the up-sample and merge operation (see Fig.4) forms a dense output having the same number of pixels of 43,520. Therefore, we ensure that the supervisions for the losses are equivalent³ for both methods.

The main difference between Naive Dense TransCenter and TransCenter is the queries: the proposed multi-scale dense queries are related to the image (from M_t) where one query represents one pixel. The benefit of image-related pixel-level queries is 3-fold: 1) with the change of input size, our dense queries can automatically adapt to the same image size without retraining; 2) Since in our case, one query is attached to one pixel

3. The Gaussian supervision in TransCenter for negative examples has values very close to 0, thus similar to the classification loss in Naive Dense TransCenter.

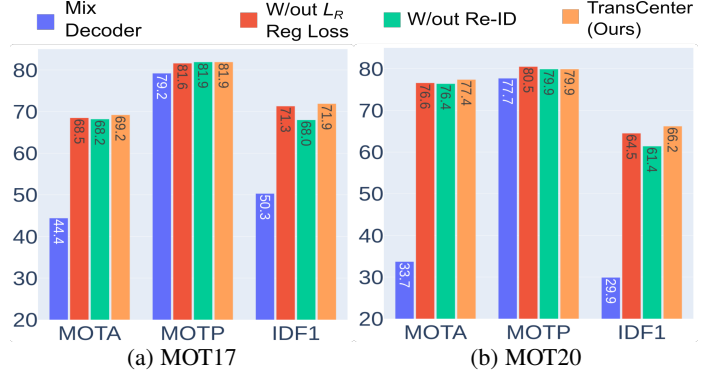


Fig. 6: Effectiveness of different components of TransCenter in MOTA, MOTP and IDF1 tested on MOT17 and MOT20 validation sets.

TABLE 4: Effectiveness of different components of TransCenter tested on MOT17 and MOT20 in FP, FN and IDS.

Method	MOT17			MOT20		
	FP ↓	FN ↓	IDS ↓	FP ↓	FN ↓	IDS ↓
Mix Decoder	305	12,991	1,782	2,888	172,624	28,682
W/out L_R Loss	1,279	7,090	184	10,381	59,803	1,719
W/out Re-ID	1,202	6,951	467	10,857	57,106	4,766
TransCenter (ours)	1,202	6,951	203	10,896	57,145	1,651

and one pixel can only be assigned to one object center (rarely the case that two object centers overlap and even, in this case, the ground-truth has to choose the foreground object), we do not need time-consuming Hungarian matching during each training step (e.g. 0.45s per training step, i.e. taking 6.9h more for training MOT20 validation set for 50 epochs.) for matching queries to the ground-truth objects. 3) the simple but naively implemented dense queries are highly overlapping (since they do not have positional mutual dependency). In spite of the one-to-one matching during training, from Tab. 3, drastically increased queries tend to predict noisier detections causing much higher FPs (+2,308 and +30,533 compared to TransCenter in MOT17 and MOT20, respectively) and thus much under-performed tracking results (-12.6% and -10.2% MOTA for MOT17 and MOT20, respectively), as shown in Fig. 5.

Mix Decoder Does Not Work We study the possibility of using a single transformer decoder and one set of dense multi-scale queries to perform both detecting and tracking simultaneously. Using a single decoder to perform both tasks leads to very poor results, as shown in Fig. 6 and Tab. 4 (Mix Decoder). This is because the decoder should pay different attention to detecting and tracking objects. Mixing the two tasks into one decoder, the network repeatedly switches its attention between image t and image $t - 1$ during training and eventually fails to detect and track objects correctly (i.e. low MOTA). Using a single decoder for sure brings the memory efficiency, which is not so crucial in TransCenter, thanks to the deformable modules [78]. The overall memory consumption is therefore affordable for a normal GPU setting (see details in Sec. 5.1).

Lost Person Re-identification We use an external Re-ID network to recover the identities which are temporally suspended by the tracker. The Re-ID network is the one in [3], pre-trained

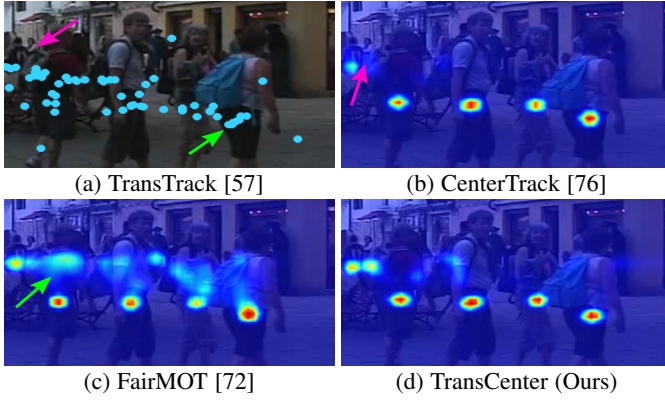


Fig. 7: Visualizations of results of state-of-the-art MOT methods: (a) shows the bounding-box centers from the queries in TransTrack; (b), (c) and (d) are center heatmaps of CenterTrack, FairMOT and TransCenter (Ours), respectively.

on MOT17 training set. Similarly, a light-weight optical flow estimation network LiteFlowNet [28] pre-trained on KITTI [19] is used to recover the lost identities. This process helps us to reduce IDS, but the overall tracking performance does not come from these external networks since FP, FN is not improved by them. From Tab. 4, we even observe a slight increase of FP and FN since the external networks were not finetuned on MOT20 person identities.

Without L_R We evaluate the impact of the additional bounding box regression loss L_R that completes the sparse object size loss, as discussed in Section 4.5. We observe a slight performance drop (-0.7% MOTA for MOT17 and -0.8% for MOT20), indicating that the two sparse regression losses and the dense center heatmap focal loss are sufficient to train TransCenter.

5.5 Qualitative Results and Visualizations

In this section, we qualitatively show the heatmap responses, the attention maps from the transformers in TransCenter and also some tracking results in very crowded scenes MOT20.

Heatmap Response We qualitatively visualize and compare our heatmap response in Fig. 7(d) with other two center heatmap-based MOT methods [72], [76] in Fig. 7(c) and Fig. 7(b) as well as the box centers predicted from sparse queries from one concurrent transformer-based MOT method [57] in Fig. 7(a).

Two *concurrent* transformer-based MOT methods [42], [57] both use sparse queries, leading to miss detections (pink arrow), that are heavily overlapped, possibly leading to false detections (green arrow). Previous MOT center trackers [72], [76] suffer from the same problems because the centers are estimated independently of each other. TransCenter is designed to mitigate these two adverse effects by using dense (pixel-level) multi-scale queries to enable heatmap-based inference and exploiting the attention mechanisms to introduce co-dependency between center predictions.

Attention Visualization We show in Fig. 8 the attention from different attention heads of both detection and tracking decoders. We can see that for the detection attention, different heads focus on different areas of I_t : (a) the people; (b), (c) the background; (d) both the background and the people. For the tracking attention, interestingly we observe that the object information at t does correlate to the previous image: in tracking (b)-(d), the tracking

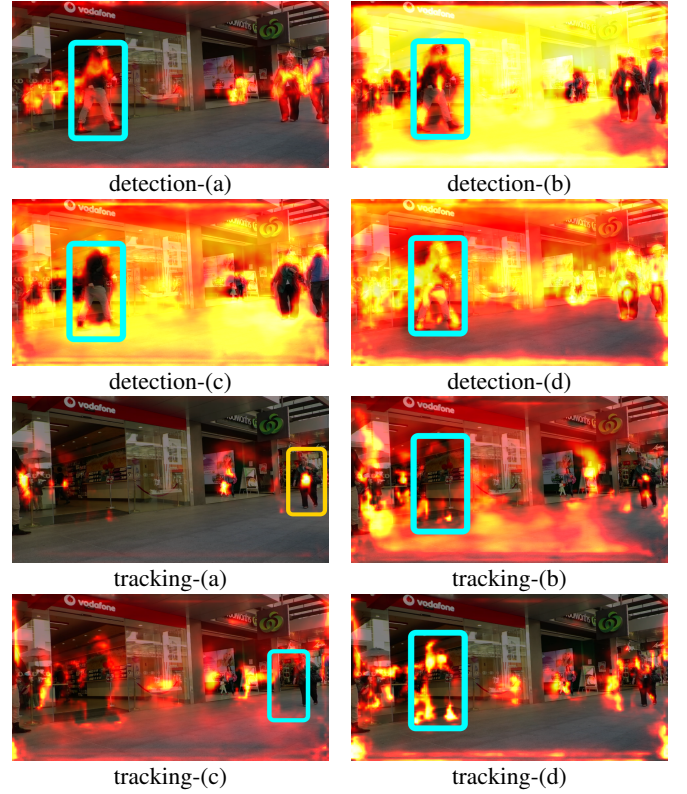


Fig. 8: Visualizations of the attention from the detection decoder and the tracking decoder in the current and previous image at $t-50$ (for better visualization), respectively. The brighter the higher the attention weights.

decoder tries to look for objects at $t-1$ in the surrounding of the positions of the objects at t . In addition, it also focuses on the objects in the previous image, as shown within the orange box in tracking-(a).

Qualitative Results We report in Fig. 9 qualitative results on the MOT20 testset, to assess the ability of TransCenter to detect and track targets in the context of crowded scenes where we show the predicted their center trajectories and the corresponding box sizes forming the highly overlapping bounding boxes. Fig. 9(a) is extracted from MOT20-04, Fig. 9(b) from MOT20-07 and Fig. 9(c) from MOT20-06. We observe that TransCenter manages to keep high recall, even in the context of drastic mutual-occlusions, and reliably associate detections across time. To summarize, TransCenter exhibits outstanding results on both MOT17 and MOT20 datasets for both public and private detections, and for both with or without extra training data, which indicates that multiple-object center point tracking using transformers is a promising research direction.

6 CONCLUSION

In this paper, we introduce TransCenter, a novel transformer-based architecture for multiple-object tracking. TransCenter proposed the use of dense pixel-level multi-scale queries in combination with a fully deformable dual decoder, able to output dense representations for the objects' center, size, and temporal displacement. The deformable decoder allows processing thousands of queries while keeping the overall memory usage within reasonable boundaries. Under the same training conditions, TransCenter

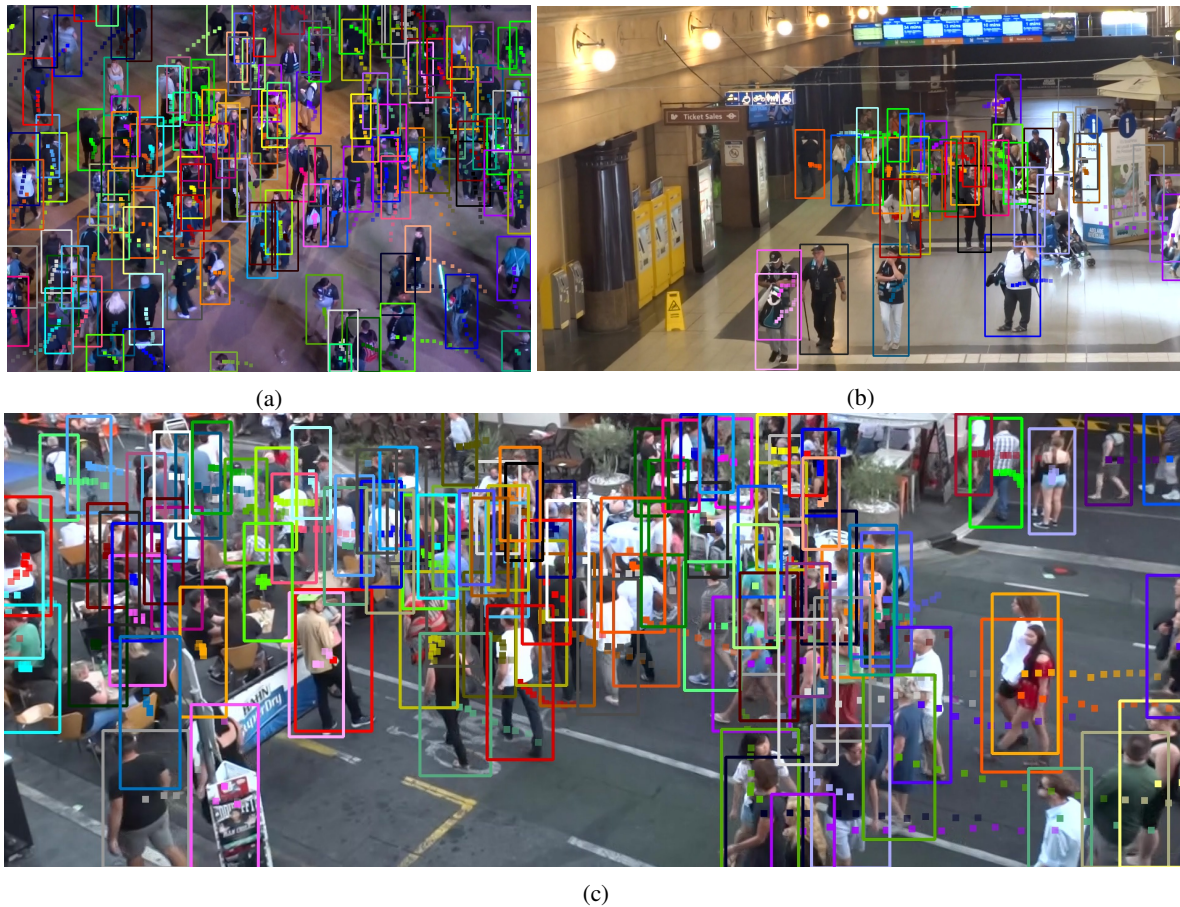


Fig. 9: Tracking trajectories visualization of very crowded scenes in MOT20 testset under the Private Detection setting.

outperforms all its competitors in MOT17 and MOT20, and even exhibits better performance to some methods trained with much more data.

REFERENCES

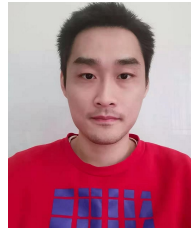
- [1] Nathanael L Baisa. Online multi-object visual tracking using a gm-phd filter with deep appearance learning. In *22th International Conference on Information Fusion (FUSION)*, pages 1–8. IEEE, 2019. 2
- [2] Yutong Ban, Sileye Ba, Xavier Alameda-Pineda, and Radu Horaud. Tracking multiple persons based on a variational bayesian model. In *European Conference on Computer Vision (ECCV)*, pages 52–67. Springer, October, 2016. 1, 2
- [3] Philipp Bergmann, Tim Meinhardt, and Laura Leal-Taixe. Tracking without bells and whistles. In *IEEE International Conference on Computer Vision (ICCV)*, pages 941–951. IEEE, October, 2019. 1, 2, 3, 4, 6, 7, 8
- [4] Keni Bernardin and Rainer Stiefelhofen. Evaluating multiple object tracking performance: the clear mot metrics. *EURASIP Journal on Image and Video Processing*, 2008:1–10, 2008. 6
- [5] Alex Bewley, Zongyuan Ge, Lionel Ott, Fabio Ramos, and Ben Uppcroft. Simple online and realtime tracking. In *IEEE international Conference on Image Processing (ICIP)*, pages 3464–3468. IEEE, September, 2016. 7
- [6] Guillem Brasó and Laura Leal-Taixé. Learning a neural solver for multiple object tracking. In *IEEE Conference on Computer Vision and Pattern Recognition (CVPR)*, pages 5247–6257. IEEE, June, 2020. 2
- [7] Nicolas Carion, Francisco Massa, Gabriel Synnaeve, Nicolas Usunier, Alexander Kirillov, and Sergey Zagoruyko. End-to-end object detection with transformers. In *European Conference on Computer Vision (ECCV)*, pages 213–229. Springer, August, 2020. 1, 2, 3
- [8] Long Chen, Haizhou Ai, Zijie Zhuang, and Chong Shang. Real-time multiple people tracking with deeply learned candidate selection and person re-identification. In *IEEE International Conference on Multimedia and Expo (ICME)*, pages 1–6. IEEE, July, 2018. 6
- [9] Jifeng Dai, Haozhi Qi, Yuwen Xiong, Yi Li, Guodong Zhang, Han Hu, and Yichen Wei. Deformable convolutional networks. In *IEEE International Conference on Computer Vision (ICCV)*, pages 764–773. IEEE, October, 2017. 2, 4, 5
- [10] Patrick Dendorfer, Hamid Rezaatofghi, Anton Milan, Javen Shi, Daniel Cremers, Ian Reid, Stefan Roth, Konrad Schindler, and Laura Leal-Taixé. Mot20: A benchmark for multi object tracking in crowded scenes. *arXiv preprint arXiv:2003.09003[cs]*, March, 2020. 1, 2, 6
- [11] Jia Deng, Wei Dong, Richard Socher, Li-Jia Li, Kai Li, and Li Fei-Fei. ImageNet: A Large-Scale Hierarchical Image Datasbet. In *IEEE Conference on Computer Vision and Pattern Recognition (CVPR)*, pages 248–255. IEEE, June, 2009. 6
- [12] Piotr Dollár, Christian Wojek, Bernt Schiele, and Pietro Perona. Pedestrian detection: A benchmark. In *IEEE Conference on Computer Vision and Pattern Recognition (CVPR)*, pages 304–311. IEEE, June, 2009. 6
- [13] Piotr Dollár, Christian Wojek, Bernt Schiele, and Pietro Perona. Pedestrian detection: An evaluation of the state of the art. *IEEE Transactions on Pattern Analysis and Machine Intelligence*, vol 34, No.4, pages 743–761. IEEE, 2011. 6
- [14] Alexey Dosovitskiy, Lucas Beyer, Alexander Kolesnikov, Dirk Weissenborn, Xiaohua Zhai, Thomas Unterthiner, Mostafa Dehghani, Matthias Minderer, Georg Heigold, Sylvain Gelly, Jakob Uszkoreit, and Neil Houlsby. An image is worth 16x16 words: Transformers for image recognition at scale. *arXiv preprint arXiv:2010.11929*, October, 2020. 2
- [15] Andreas Ess, Bastian Leibe, Konrad Schindler, and Luc van Gool. A mobile vision system for robust multi-person tracking. In *IEEE Conference on Computer Vision and Pattern Recognition (CVPR)*, pages 1–8. IEEE, June, 2008. 6
- [16] Chuang Gan, Deng Huang, Peihao Chen, Joshua B Tenenbaum, and Antonio Torralba. Foley music: Learning to generate music from videos. *European Conference on Computer Vision (ECCV)*, pages 758–775. Springer, August, 2020. 2
- [17] Chuang Gan, Deng Huang, Hang Zhao, Joshua B Tenenbaum, and Antonio Torralba. Music gesture for visual sound separation. In *IEEE Conference on Computer Vision and Pattern Recognition (CVPR)*, pages 10478–10487. IEEE, June, 2020. 2

- [18] Chuang Gan, Hang Zhao, Peihao Chen, David Cox, and Antonio Torralba. Self-supervised moving vehicle tracking with stereo sound. In *IEEE International Conference on Computer Vision (ICCV)*, pages 7053–7062. IEEE, October, 2019. 1
- [19] Andreas Geiger, Philip Lenz, and Raquel Urtasun. Are we ready for autonomous driving? the kitti vision benchmark suite. In *IEEE Conference on Computer Vision and Pattern Recognition (CVPR)*, pages 3354–3361. IEEE, June, 2012. 9
- [20] Song Guo, Jingya Wang, Xinchao Wang, and Dacheng Tao. Online Multiple Object Tracking with Cross-Task Synergy. In *IEEE Conference on Computer Vision and Pattern Recognition (CVPR)*, pages 8136–8145. IEEE, June, 2021. 2, 6, 7
- [21] Shoudong Han, Piao Huang, Hongwei Wang, En Yu, Donghaisheng Liu, Xiaofeng Pan, and Jun Zhao. Mat: Motion-aware multi-object tracking. *arXiv preprint arXiv:2009.04794*, September, 2020. 2, 6
- [22] Jiawei He, Zehao Huang, Naiyan Wang, and Zhaoxiang Zhang. Learnable Graph Matching: Incorporating Graph Partitioning with Deep Feature Learning for Multiple Object Tracking. In *IEEE Conference on Computer Vision and Pattern Recognition (CVPR)*, pages 5299–5309. IEEE, June, 2021. 2, 6
- [23] Kaiming He, Xiangyu Zhang, Shaoqing Ren, and Jian Sun. Deep residual learning for image recognition. In *IEEE conference on computer vision and pattern recognition (CVPR)*, pages 770–778. IEEE, June, 2016. 2, 3, 6
- [24] Lingxiao He and Wu Liu. Guided saliency feature learning for person re-identification in crowded scenes. In *European Conference on Computer Vision (ECCV)*, pages 357–373. Springer, October, 2020. 1
- [25] Lingxiao He, Yinggang Wang, Wu Liu, He Zhao, Zhenan Sun, and Jiashi Feng. Foreground-aware pyramid reconstruction for alignment-free occluded person re-identification. In *IEEE International Conference on Computer Vision (ICCV)*, pages 8450–8459. IEEE, October, 2019. 1
- [26] Shuting He, Hao Luo, Pichao Wang, Fan Wang, Hao Li, and Wei Jiang. Transreid: Transformer-based object re-identification. *arXiv preprint arXiv:2102.04378*, February, 2021. 1, 2
- [27] Andrea Hornakova, Roberto Henschel, Bodo Rosenhahn, and Paul Swo-boda. Lifted disjoint paths with application in multiple object tracking. In *International Conference on Machine Learning (ICML)*, pages 4364–4375. PMLR, July, 2020. 2
- [28] Tak-Wai Hui, Xiaou Tang, and Chen Change Loy. Liteflownet: A lightweight convolutional neural network for optical flow estimation. In *IEEE Conference on Computer Vision and Pattern Recognition (CVPR)*, pages 8981–8989. IEEE, June, 2018. 9
- [29] Yifan Jiang, Shiyu Chang, and Zhangyang Wang. Transgan: Two transformers can make one strong gan. *arXiv preprint arXiv:2102.07074*, February, 2021. 2
- [30] Shyamgopal Karthik, Ameya Prabhu, and Vineet Gandhi. Simple unsupervised multi-object tracking. *arXiv preprint arXiv:2006.02609*, June, 2020. 6, 7
- [31] Margret Keuper, Siyu Tang, Yu Zhongjie, Bjoern Andres, Thomas Brox, and Bernt Schiele. A multi-cut formulation for joint segmentation and tracking of multiple objects. *arXiv preprint arXiv:1607.06317*, July, 2016. 2
- [32] Chanho Kim, Fuxin Li, Mazen Alotaibi, and James M Rehg. Discriminative Appearance Modeling with Multi-track Pooling for Real-time Multi-object Tracking. In *IEEE Conference on Computer Vision and Pattern Recognition (CVPR)*, pages 9553–9562. IEEE, June, 2021. 6
- [33] Hei Law and Jia Deng. Cornernet: Detecting objects as paired keypoints. In *European Conference on Computer Vision (ECCV)*, pages 734–750. Springer, September, 2018. 2, 5
- [34] Wei Li, Rui Zhao, Tong Xiao, and Xiaogang Wang. Deepreid: Deep filter pairing neural network for person re-identification. In *IEEE Conference on Computer Vision and Pattern Recognition (CVPR)*, pages 152–159. IEEE, June, 2014. 6
- [35] Yuan Li, Chang Huang, and Ram Nevatia. Learning to associate: Hybridboosted multi-target tracker for crowded scene. In *IEEE Conference on Computer Vision and Pattern Recognition (CVPR)*, pages 2953–2960. IEEE, June, 2009. 6
- [36] Chao Liang, Zhipeng Zhang, Yi Lu, Xue Zhou, Bing Li, Xiyong Ye, and Jianxiao Zou. Rethinking the competition between detection and reid in multi-object tracking. *arXiv preprint arXiv:2010.12138*, October, 2020. 6, 7
- [37] Matthieu Lin, Chuming Li, Xingyuan Bu, Ming Sun, Chen Lin, Junjie Yan, Wanli Ouyang, and Zhidong Deng. Detr for pedestrian detection. *arXiv preprint arXiv:2012.06785*, December, 2020. 1
- [38] Tsung-Yi Lin, Michael Maire, Serge Belongie, James Hays, Pietro Perona, Deva Ramanan, Piotr Dollár, and C Lawrence Zitnick. Microsoft coco: Common objects in context. In *European Conference on Computer Vision (ECCV)*, pages 740–755. Springer, August, 2014. 6
- [39] Qiankun Liu, Qi Chu, Bin Liu, and Nenghai Yu. Gsm: Graph similarity model for multi-object tracking. In Christian Bessiere, editor, *Proceedings of the Twenty-Ninth International Joint Conference on Artificial Intelligence (IJCAI)*, pages 530–536. International Joint Conferences on Artificial Intelligence Organization, July, 2020. Main track. 6
- [40] Ilya Loshchilov, and Frank Hutter. Decoupled weight decay regularization. *International Conference on Learning Representations (ICLR)*, May, 2019. 6
- [41] Santiago Manen, Michael Gygli, Dengxin Dai, and Luc Van Gool. Pathtrack: Fast trajectory annotation with path supervision. In *IEEE International Conference on Computer Vision (ICCV)*, pages 290–299. IEEE, October, 2017. 6
- [42] Tim Meinhardt, Alexander Kirillov, Laura Leal-Taixe, and Christoph Feichtenhofer. Trackformer: Multi-object tracking with transformers. *arXiv preprint arXiv:2101.02702*, January, 2021. 1, 3, 4, 6, 7, 9
- [43] Anton Milan, Laura Leal-Taixe, Ian Reid, Stefan Roth, and Konrad Schindler. MOT16: A benchmark for multi-object tracking. *arXiv preprint arXiv:1603.00831 [cs]*, March, 2016. 1, 2, 6
- [44] Anton Milan, Seyed Hamid Rezaatoughi, Anthony Dick, Ian Reid, and Konrad Schindler. Online multi-target tracking using recurrent neural networks. In *AAAI Conference on Artificial Intelligence*, vol 31. AAAI, February, 2017. 2
- [45] Jiangmiao Pang, Linlu Qiu, Xia Li, Haofeng Chen, Qi Li, Trevor Darrell, and Fisher Yu. Quasi-dense similarity learning for multiple object tracking. In *IEEE Conference on Computer Vision and Pattern Recognition (CVPR)*, pages 164–173. IEEE, June, 2021. 2, 6
- [46] Ioannis Papakis, Abhijit Sarkar, and Anuj Karpatne. Gcnmatch: Graph convolutional neural networks for multi-object tracking via sinkhorn normalization. *arXiv preprint arXiv:2010.00067*, September, 2020. 2, 7
- [47] Jinlong Peng, Changan Wang, Fangbin Wan, Yang Wu, Yabiao Wang, Ying Tai, Chengjie Wang, Jilin Li, Feiyue Huang, and Yanwei Fu. Chained-tracker: Chaining paired attentive regression results for end-to-end joint multiple-object detection and tracking. In *European Conference on Computer Vision (ECCV)*, pages 145–161. Springer, August, 2020. 1, 6
- [48] Ren Shaoqing, He Kaiming, Girshick Ross and Sun Jian. Faster r-cnn: Towards real-time object detection with region proposal networks. In *Advances in neural information processing systems (NeurIPS)*, vol 28, pages 91–99. December, 2015. 2
- [49] Redmon Joseph, Divvala Santosh, Girshick Ross and Farhadi Ali. Faster r-cnn: Towards real-time object detection with region proposal networks. In *IEEE Conference on Computer Vision and Pattern Recognition (CVPR)*, pages 779–788. IEEE, June, 2016. 2
- [50] Seyed Hamid Rezaatoughi, Anton Milan, Zhen Zhang, Qinfeng Shi, Anthony Dick, and Ian Reid. Joint probabilistic data association revisited. In *IEEE International Conference on Computer Vision (ICCV)*, pages 3047–3055. IEEE, December, 2015. 1, 2
- [51] Ergys Ristani, Francesco Solera, Roger Zou, Rita Cucchiara, and Carlo Tomasi. Performance measures and a data set for multi-target, multi-camera tracking. In *European Conference on Computer Vision (ECCV)*, pages 17–35. Springer, October, 2016. 6
- [52] Amir Sadeghian, Alexandre Alahi, and Silvio Savarese. Tracking the untrackable: Learning to track multiple cues with long-term dependencies. In *IEEE International Conference on Computer Vision (ICCV)*, pages 300–311. IEEE, October, 2017. 2
- [53] Fatemeh Saleh, Sadegh Aliakbarian, Hamid Rezaatoughi, Mathieu Salzmann, and Stephen Gould. Probabilistic Tracklet Scoring and Inpainting for Multiple Object Tracking. In *IEEE Conference on Computer Vision and Pattern Recognition (CVPR)*, pages 14329–14339. IEEE, June, 2021. 2, 6, 7
- [54] Chaobing Shan, Chunbo Wei, Bing Deng, Jianqiang Huang, Xian-Sheng Hua, Xiaoliang Cheng, and Kewei Liang. Tracklets predicting based adaptive graph tracking. *arXiv preprint arXiv:2010.09015*, October, 2020. 1, 6
- [55] Shuai Shao, Zijian Zhao, Boxun Li, Tete Xiao, Gang Yu, Xiangyu Zhang, and Jian Sun. Crowdhuman: A benchmark for detecting human in a crowd. *arXiv preprint arXiv:1805.00123*, April, 2018. 6
- [56] Bing Shuai, Andrew Berneshawi, Xinyu Li, Davide Modolo, and Joseph Tighe. SiamMOT: Siamese Multi-Object Tracking. In *IEEE Conference on Computer Vision and Pattern Recognition (CVPR)*, pages 12372–12382. IEEE, June, 2021. 2, 6
- [57] Peize Sun, Yi Jiang, Rufeng Zhang, Enze Xie, Jinkun Cao, Xint-ing Hu, Tao Kong, Zehuan Yuan, Changhu Wang, and Ping Luo. Transtrack: Multiple-object tracking with transformer. *arXiv preprint arXiv:2012.15460*, December, 2020. 3, 4, 6, 7, 9
- [58] Siyu Tang, Bjoern Andres, Miykhaylo Andriluka, and Bernt Schiele. Subgraph decomposition for multi-target tracking. In *IEEE Conference on Computer Vision and Pattern Recognition (CVPR)*, pages 5033–5041. IEEE, June, 2015. 2
- [59] Siyu Tang, Bjoern Andres, Miykhaylo Andriluka, and Bernt Schiele. Multi-person tracking by multicut and deep matching. In *European*

- Conference on Computer Vision (ECCV)*, pages 100–111. Springer, October, 2016. 2
- [60] Siyu Tang, Mykhaylo Andriluka, Bjoern Andres, and Bernt Schiele. Multiple people tracking by lifted multicut and person re-identification. In *IEEE Conference on Computer Vision and Pattern Recognition (CVPR)*, pages 3539–3548. IEEE, July, 2017. 2
- [61] Ashish Vaswani, Noam Shazeer, Niki Parmar, Jakob Uszkoreit, Llion Jones, Aidan N Gomez, Lukasz Kaiser, and Illia Polosukhin. Attention is all you need. *Neural Information Processing Systems (NeurIPS)*, pages 5998–6008. June, 2017. 1, 2, 5
- [62] Jialian Wu, Jiale Cao, Liangchen Song, Yu Wang, Ming Yang, and Junsong Yuan. Track to Detect and Segment: An Online Multi-Object Tracker. In *IEEE Conference on Computer Vision and Pattern Recognition (CVPR)*, pages 12352–12361. IEEE, June, 2021. 2, 6
- [63] Qiang Wang, Yun Zheng, Pan Pan, and Yinghui Xu. Multiple Object Tracking with Correlation Learning. In *IEEE Conference on Computer Vision and Pattern Recognition (CVPR)*, pages 3876–3886. IEEE, June, 2021. 2, 6, 7
- [64] Yongxin Wang, Kris Kitani, and Xinshuo Weng. Joint object detection and multi-object tracking with graph neural networks. *IEEE International Conference on Robotics and Automation (ICRA)*. IEEE, May, 2021. 1, 2, 6, 7
- [65] Xinshuo Weng, Yongxin Wang, Yunze Man, and Kris M Kitani. Gnn3dmot: Graph neural network for 3d multi-object tracking with 2d-3d multi-feature learning. In *IEEE Conference on Computer Vision and Pattern Recognition (CVPR)*, pages 6499–6508. IEEE, June, 2020. 2
- [66] Xinshuo Weng, Ye Yuan, and Kris Kitani. Joint 3d tracking and forecasting with graph neural network and diversity sampling. *arXiv preprint arXiv:2003.07847*, March, 2020. 2
- [67] Tong Xiao, Shuang Li, Bochao Wang, Liang Lin, and Xiaogang Wang. Joint Detection and Identification Feature Learning for Person Search. *arXiv preprint arXiv:1604.01850*, April, 2016. 6
- [68] Yihong Xu, Aljosa Osep, Yutong Ban, Radu Horaud, Laura Leal-Taixé, and Xavier Alameda-Pineda. How to train your deep multi-object tracker. In *IEEE Conference on Computer Vision and Pattern Recognition (CVPR)*, pages 6787–6796. IEEE, June, 2020. 1, 2, 3, 4, 6
- [69] Fuzhi Yang, Huan Yang, Jianlong Fu, Hongtao Lu, and Baining Guo. Learning texture transformer network for image super-resolution. In *IEEE Conference on Computer Vision and Pattern Recognition (CVPR)*, pages 5791–5800. IEEE, June, 2020. 1, 2
- [70] Shanshan Zhang, Rodrigo Benenson, and Bernt Schiele. Citypersons: A diverse dataset for pedestrian detection. In *IEEE Conference on Computer Vision and Pattern Recognition (CVPR)*, pages 3213–3221. IEEE, July, 2017. 6
- [71] Yang Zhang, Hao Sheng, Yubin Wu, Shuai Wang, Wei Ke, and Zhang Xiong. Multiplex labeling graph for near-online tracking in crowded scenes. *IEEE Internet of Things Journal*, 7(9):7892–7902. IEEE, May, 2020. 1, 6, 7
- [72] Yifu Zhang, Chunyu Wang, Xinggang Wang, Wenjun Zeng, and Wenyu Liu. Fairmot: On the fairness of detection and re-identification in multiple object tracking. *arXiv preprint arXiv:2004.01888*, April, 2020. 1, 2, 3, 5, 6, 7, 9
- [73] Linyu Zheng, Ming Tang, Yingying Chen, Guibo Zhu, Jinqiao Wang, and Hanqing Lu. Improving Multiple Object Tracking With Single Object Tracking. In *IEEE Conference on Computer Vision and Pattern Recognition (CVPR)*, pages 2453–2462. IEEE, June, 2021. 1, 2, 3, 6, 7
- [74] Liang Zheng, Liyue Shen, Lu Tian, Shengjin Wang, Jingdong Wang, and Qi Tian. Scalable person re-identification: A benchmark. In *IEEE International Conference on Computer Vision (ICCV)*, pages 1116–1124. IEEE, December, 2015. 6
- [75] Liang Zheng, Hengheng Zhang, Shaoyan Sun, Manmohan Chandraker, Yi Yang, and Qi Tian. Person re-identification in the wild. In *IEEE Conference on Computer Vision and Pattern Recognition (CVPR)*, pages 1367–1376. IEEE, July, 2017. 6
- [76] Xingyi Zhou, Vladlen Koltun, and Philipp Krähenbühl. Tracking objects as points. In *European Conference on Computer Vision (ECCV)*, pages 474–490. Springer, August, 2020. 1, 2, 3, 5, 6, 7, 9
- [77] Xingyi Zhou, Dequan Wang, and Philipp Krähenbühl. Objects as points. *arXiv preprint arXiv:1904.07850*, 2020. 2
- [78] Xizhou Zhu, Weijie Su, Lewei Lu, Bin Li, Xiaogang Wang, and Jifeng Dai. Deformable detr: Deformable transformers for end-to-end object detection. *arXiv preprint arXiv:2010.04159*, 2020. 1, 2, 3, 4, 5, 8

ACKNOWLEDGMENTS

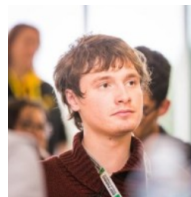
Xavier Alameda-Pineda acknowledges funding from the ANR ML3RI project (ANR-19-CE33-0008-01) and the H2020 SPRING project (under GA #871245).



Yihong Xu is currently a third-year Ph.D. student in the RobotLearn team at Inria Grenoble Rhône-Alpes. Previously, he received his master's degree from IMT Atlantique (previously Télécom Bretagne). His research interests lie in multiple-object tracking applications using machine learning.



Yutong Ban Yutong Ban is currently a postdoctoral research fellow at both Distributed Robotics Lab, CSAIL, MIT and Surgical Artificial Intelligence, MGH. He received the BSc degree in telecommunications from Xidian University, China, and the engineering degree in image processing and computer science from Telecom Saint-Etienne, France. He received his Ph.D. degree with the PERCEPTION team at INRIA Grenoble Rhône-Alpes and University Grenoble Alpes. His research interests include surgical video analysis, audio-visual cross-modal learning, and multi-object tracking.



Guillaume Delorme is a Ph.D. student in the RobotLearn team at Inria Grenoble Rhône-Alpes since September 2017. He received an engineering degree in applied mathematics and computer science from the Ensimag Institut Polytechnique de Grenoble in 2017. He is especially interested in deep learning, appearance modeling, person re-identification, and visual tracking.



Chuang Gan is a principal research staff member at MIT-IBM Watson AI Lab. He is also an affiliated researcher at MIT EECS. His research interests focus on computer vision and machine learning. His research works have been recognized by Microsoft Fellowship, Baidu Fellowship, and media coverage from CNN, BBC, The New York Times, WIRED, Forbes, and MIT Tech Review. He has also served as an area chair of CVPR, ICCV, ACL, ICLR, and an associate editor of IEEE Transactions on Image Processing and IEEE Transactions on Circuits and Systems for Video Technology.



Daniela Rus (Fellow, IEEE) received the Ph.D. degree in computer science from Cornell University, Ithaca, NY, USA, in 1993. She is the Andrew (1956) and Erna Viterbi Professor of Electrical Engineering and Computer Science and the Director of the Computer Science and Artificial Intelligence Laboratory with Massachusetts Institute of Technology (MIT), Cambridge, MA, USA. Prior to joining MIT, she was a Professor with the Department of Computer Science, Dartmouth College, Hanover, NH, USA. Her research interests include robotics, mobile computing, and big data.

The key focus of her research is to develop the science of networked/distributed/collaborative robotics. Dr. Rus is a Class of 2002 MacArthur Fellow, a Fellow of ACM and AAAI, and a member of the National Academy of Engineering.



Xavier Alameda-Pineda is a (tenured) Research Scientist at Inria, and the Leader of the RobotLearn Team. He obtained the M.Sc. (equivalent) in Mathematics in 2008, in Telecommunications in 2009 from BarcelonaTech, and in Computer Science in 2010 from Université Grenoble-Alpes (UGA). He then worked towards his Ph.D. in Mathematics and Computer Science, and obtained it in 2013, from UGA. After a two-year post-doc period at the Multimodal Human Understanding Group, at the University of Trento, he was appointed with his current position. Xavier is an active member of SIGMM, a senior member of IEEE, and a member of ELLIS. He is the Coordinator of the H2020 Project SPRING: Socially Pertinent Robots in Gerontological Healthcare and is co-leading the “Audio-visual machine perception and interaction for companion robots” chair of the Multidisciplinary Institute of Artificial Intelligence. Xavier’s research interests are in combining machine learning, computer vision, and audio processing for scene and behavior analysis and human-robot interaction.